Optical studies of vertical ambipolar transport and interface recombination velocities in GaAs/$Al_{0.5}Ga_{0.5}As$ double-quantum-well heterostructures

H. Hillmer* and A. Forchel†
4. Physikalisches Institut, Universität Stuttgart, Pfaffenwaldring 57, D-7000 Stuttgart, Germany

T. Kuhn‡ and G. Mahler
Institut für Theoretische Physik, Universität Stuttgart, Pfaffenwaldring 57, D-7000 Stuttgart, Germany

H. P. Meier
IBM Research Division, Forschungslabor Zürich, CH-8803 Rüschlikon, Switzerland
(Received 6 November 1990; revised manuscript received 19 February 1991)

We present a detailed experimental and theoretical study of vertical ambipolar transport in semiconductor heterostructures. A high-resolution time-of-flight method using two vertically separated quantum wells of different well widths is applied to probe the carrier transport perpendicular to the heterointerfaces. By a numerical simulation the ambipolar diffusivities as well as surface and interface recombination velocities in GaAs/$Al_xGa_{1-x}As$ structures are determined. This paper emphasizes the importance of surface and interface recombination for the analysis of the transport data. Alloy-disorder scattering is found to limit the ambipolar mobilities between 40 and 120 K in the $Al_{0.5}Ga_{0.5}As$ barriers with acoustic-deformation-potential and polar-optical scattering participating above 120 K. In addition to the transport properties, we also obtain information on carrier capture from the barrier layers into the quantum well as a function of temperature.

I. INTRODUCTION

Studies of carrier transport perpendicular to heterointerfaces have attracted considerable interest due to the related physics and their device application. Various experimental methods have been used: Carrier pairs have been generated by short laser pulses at one interface of a graded heterostructure and the carrier-induced reflectivity change at the opposite interface of the grading has been studied.[1] To determine electron and hole mobilities in superlattices (SL's), heterostructure transistors including a SL base were investigated.[2] Carrier separation at *p-n* junction was used to probe minority-carrier diffusion and to determine diffusion lengths.[3] The methods reported in Refs. 1 and 3 illustrate typical time-of-flight arrangements in which the position where the carriers are generated is spatially separated from a position inside the sample, where the carriers are probed after traveling across the flight distance.

In order to improve the spatial resolution in vertical time-of-flight (TOF) studies, ultrathin probe layers, e.g., quantum wells[4–10] (QW's) with specific spectral behavior have been integrated in the structures at the end of the studied transport distance. Ambipolar carrier transport was studied in GaAs/$Al_xGa_{1-x}As$ (Ref. 5) and $In_{1-z}Ga_xAs$/InP (Ref. 7) using our TOF method[5] by time-resolved spectroscopy. An enlarged well terminating an SL sequence was used to investigate ambipolar perpendicular transport in graded GaAs/$Al_xGa_{1-x}As$ SL's by time-resolved[6,8–10] and time-integrated[4,9] spectroscopy. However, in all these studies[4–10] including ours[5] the influence on transport by the QW's used for probing the carrier motion is more or less neglected. In order to fit our experimental profiles in Ref. 5, e.g., we phenomenologically introduced an "expansion velocity" via a drift term in the diffusion equation. From the evaluation presented here this velocity is a rough approximation to the surface and interface influence in heterostructures. Previously, the influence of boundary conditions was studied theoretically in a kinetic and hydrodynamic approach.[11–13]

If, e.g., surface recombination is neglected for surface-generated carriers the maximum of the concentration profile is located at the surface for all times. Using a finite surface recombination velocity, the carrier concentration is reduced at the surface, which causes a shift of the profile maximum into the sample. An "expansion velocity" also shifts the concentration maximum from the surface into the bulk and also effectively reduces the carrier lifetime inside the system. From a theoretical point of view, however, there are important differences since the concentration maximum does not move with a constant velocity.

Theoretical studies concerning the process of carrier capture by a QW have been performed using different microscopic models, e.g., emission of optical phonons[13–17] or electron-electron scattering,[18] either using initial states which are unperturbed by the presence of the QW (Refs. 16 and 18) or taking into account quantum-mechanical resonances due to virtual bound states in the continuum.[13–15,17] Experimentally, the capture has been studied in separate confinement heterostructures with graded barriers of different shape[19–23] as well as in QW's with ungraded barriers.[7,12,16,17,24–27]

In this paper we report experimental and theoretical studies of vertical transport in GaAs/$Al_xGa_{1-x}As$ heterostructures in which the surface and interface influence has been taken into account in detail. The basic features of our TOF method are described below and were published previously.[5] The analysis of the experimental results is performed by an ambipolar diffusion model. Important improvements in the evaluation of the transport profiles now allow us to study a large number of physical properties relevant to the transport. Besides the determination of diffusivities in the three-dimensional heterostructure barrier layer, surface recombination velocities and interface trapping velocities are obtained. Furthermore, our method provides insight in the trapping of carriers in QW's.

II. SAMPLE DESIGN AND EXPERIMENTAL SETUP FOR VERTICAL TRANSPORT STUDIES

Figure 1 schematically displays the design of our QW heterostructures along the growth direction (z direction). Two GaAs QW's (QW1 and QW2) with different well widths L_{z1} and L_{z2} are located between $Al_{0.5}Ga_{0.5}As$ barriers of various widths d_1, d_2, and d_3. In the lower part of the diagram the band structure $E(z)$ is shown. Since the widths L_{z1} and L_{z2} are much smaller than the barrier widths d_1, d_2, and d_3 (see Table I), the extension of the QW's can be neglected for the transport in the barrier regions. Effectively, the QW's act as two-dimensional interfaces with bound localized interface states.

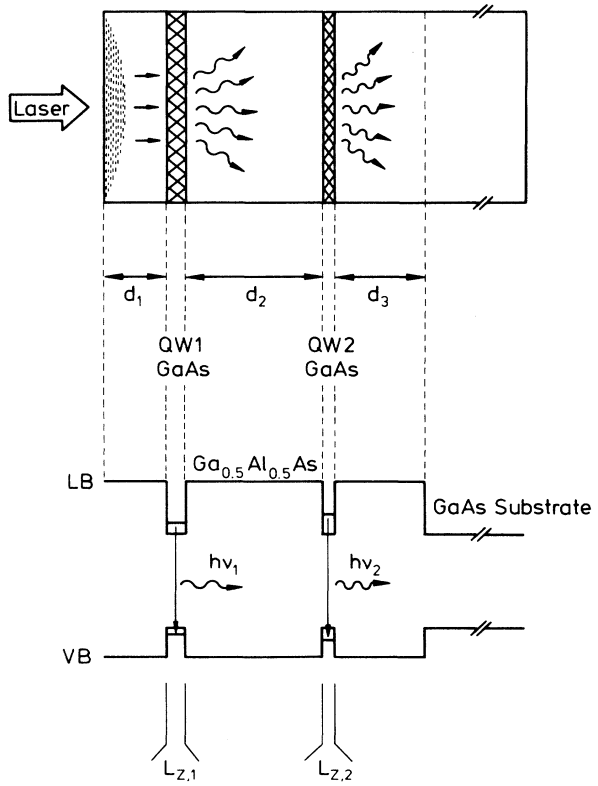

FIG. 1. Design of samples used for vertical time-of-flight studies. Top: schematic design of the samples in the x-z plane. The x direction is compressed by more than a factor of 100. Bottom: band structure along the z direction. The characteristic features are two quantum wells (QW's) of different thicknesses acting as probe layers. The arrows indicate the laser excitation and the carrier diffusion.

To limit the generation of carrier pairs mainly to the first barrier (absorption layer d_1) we use high-energetic excitation (2.41 eV). The absorption coefficient for $Al_{0.5}Ga_{0.5}As$ is about 33 000 cm^{-1} for this energy at $T=100$ K,[28,29] which yields an absorption depth of approximately 300 nm. To obtain a one-dimensional transport geometry, a laser focus diameter much larger than the sum of all barrier thicknesses d_1 is used. In Fig. 1 the lateral carrier cloud appearing immediately after the optical generation is schematically shown (dots). Some of the carrier pairs that reach QW1 are captured and indicate their position by the characteristic radiative emission of the well. In a similar way, the emission of QW2 indicates when carrier pairs have reached QW2. The different emission energies of the QW's are illustrated in Fig. 1 by different wavelengths of the emissions. QW1 is reached much earlier by the main part of the carriers than QW2 and has a lower emission energy than QW2 ($L_{z1} > L_{z2}$). This prevents a reabsorption of the emitted photons by QW2 (photon recycling).

The total number of carriers that reach QW2 is expected to be smaller than the number of carriers at QW1. Furthermore, we have chosen $L_{z1} > L_{z2}$ which in general may lead to a smaller capture rate for QW2. We therefore expect a reduced emission intensity of QW2 compared to QW1. In order to increase the emission intensity and the detection sensitivity of QW2, we used two single QW's of identical thickness of 4.2 nm separated by a 2-nm $Al_xGa_{1-x}As$ barrier in all structures. In order to simplify the description in this paper, QW2 always represents these two QW's. Note that we obtain a total thickness of QW2 which is comparable to the well width of the single QW1 in this case.

We investigated the excitation power dependence of

TABLE I. Growth parameters of the as-grown samples (Nos. 1–3) and the etched samples verified by electron micrographs, SIMS profiles, and surface profiling. All units are in nm.

Sample No.	d_1	L_{z1}	d_2	L_{z2}	d_3
1	940	10	2830	4.2	960
1a	900	10	2830	4.2	960
1b			2761	4.2	960
1c			2610	4.2	960
1d			2551	4.2	960
1e			1513	4.2	960
2	940	9.5	940	4.2	960
2a	900	9.5	940	4.2	960
2b			900	4.2	960
2c			851	4.2	960
2d			676	4.2	960
3	940	10	470	4.2	960

the emission intensity by using a high-energetic excitation (2.41 eV, generating carriers mainly inside the barriers) and a selective excitation only inside the QW's (e.g., 1.94 eV, which is smaller than the fundamental bandgap of the $Al_{0.5}Ga_{0.5}As$ barrier of 2.077 eV at 100 K). In both cases, we found that the radiative emission intensity of the QW's is directly proportional to the excitation power. Thus, the emission intensity is proportional to the concentration of carrier pairs trapped in the QW. Recording the QW emission as a function of time, we can determine the variation of the concentration of carrier pairs at the position of the QW's as a function of time.

A series of three samples Nos. 1–3 was grown on GaAs substrates by molecular-beam epitaxy. By dry etching we further generated nine different samples removing material layers of well-defined thickness from the surface of the as-grown samples. To study the influence of the surface and the interfaces as well as the influence of the QW's on transport, the thicknesses of the barrier layers d_1 and d_2 were varied (i.e., in some structures QW1 was also removed). The structure of all samples used for our studies can be found in Table I.

To obtain a high spatial resolution (< 0.1 μm), the thicknesses of all layers must be known very precisely. Therefore, the thicknesses obtained from the growth parameters were verified by electron microscope studies of cleaved samples and secondary-ion mass spectroscopy (SIMS) depth profiles.

Figure 2 shows a spectrum of a double QW structure No. 1 at $T=70$ K for 2.41 eV excitation energy. The emission of the two QW's is clearly separated. The small peaks in the low-energy part of the spectrum are due to the emission of the GaAs substrate and the superlattice buffer located near the substrate. Excitation densities (for 2.41 eV photon energy) of 25 or 2 kW/cm^2 were used which generate a concentration of carrier pairs in the absorption layer d_1 immediately after the excitation of 2×10^{17} and 1.6×10^{16} cm^{-3}, respectively. These low densities were chosen in order to avoid nonlinear saturation effects in trapping or relaxation (e.g., bottleneck effects).

The carrier pairs are generated by short light pulses of two different laser systems: a mode-locked Ar^+ laser and a synchronously mode-locked Ar^+-laser–dye-laser system (pulse width < 10 ps). The samples are mounted in a variable-temperature cryostat (1.8–300 K). The emitted photoluminescence is dispersed by a double monochromator in subtractive, i.e., chirp-compensated, alignment. The dispersed signal is detected by a fast microchannel-plate photomultiplier and processed by a fast photon counting system (total time resolution ≈ 50 ps).

III. EXPERIMENTAL TRANSPORT PROFILES AND EVALUATION BY A THEORETICAL MODEL

Prior to the transport studies characteristic transient parameters like lifetime and effective relaxation time[30] of the QW's probing the carrier motion have to be determined as a function of temperature. In order to obtain these parameters independently of transport effects, we excited the samples with energies of about 1.94 eV to generate carrier pairs only in the QW's. The evaluation of the recorded emission profiles is performed using a simple relaxation-recombination model.[30] The carriers are generated in an excited state that is determined by the excess energy of the laser pulse. The effective relaxation time τ_{rel} includes the relaxation to the first subband involving various intrasubband and intersubband relaxation mechanisms as well as an "exciton formation time."[30] The recombination is characterized by the exciton lifetime τ_w. For an excitation energy of 1.94 eV the characteristic times τ_w and τ_{rel} are displayed for QW2 in Fig. 3 as a function of temperature. The variation of τ_w as a function of temperature has been discussed already in Refs. 30–32. For temperatures exceeding about 50 K, τ_{rel} is

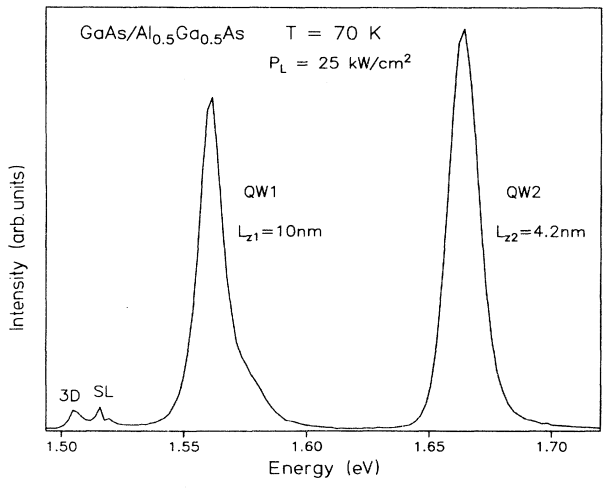

FIG. 2. Photoluminescence spectrum of a $GaAs/Al_{0.5}Ga_{0.5}As$ double-quantum-well structure (QW1 and QW2) for $T=70$ K. By high-energetic photons (2.41 eV, 25 kW/cm^2) carriers are mainly generated in the barrier located near the surface.

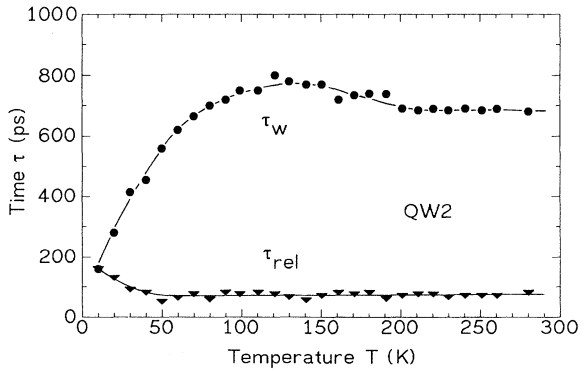

FIG. 3. Characteristic times for the carrier population of QW2 as a function of temperature: carrier lifetime τ_w (top) and effective relaxation time τ_{rel} (bottom) for sample No. 2. The solid lines are drawn to guide the eye.

found to be constant (average value 69 ps) within the experimental error [our time resolution ~50 ps (Ref. 30)]. However, for the transport studies, the carrier relaxation starts slightly higher from the band edge of the barrier material. Energy relaxation processes at these high excess energies, however, occur on a timescale of a few ps or less and can be neglected in our case.

The comparison of the time-resolved emission of a QW after excitation above (2.41 eV) and below (1.94 eV) the barrier directly visualizes the transport effects. For QW2 in structure No. 2 this is displayed in Fig. 4 at $T=50$ K. Using photon energies that excite carriers directly inside the QW (see left inset) the rise of the time-resolved emission is described by τ_{rel}. An excitation above the band gap of the barrier (see right inset) additionally involves transport processes of carriers from the position of generation to the probe layer (QW). This causes a delay in the rise of the profiles, a distinct shift of the profile peaks to longer times, a broadening of the profiles, and a prolongation of the decrease of the profiles. This behavior can be observed also for QW1 which is located near the surface. However, these effects are much weaker in this case due to a smaller distance of QW1 from the generation region compared to QW2.

Figure 5 depicts the time-resolved emission of QW1 and QW2 at $T=60$ K for a generation of carriers in the top barrier of sample No. 2. The profile of QW1 is found to increase and decrease much faster than the profile of QW2. This is due to the fact that the main part of the carrier cloud reaches the first probe layer much earlier than the second one. The main difference between the two profiles is caused by the carrier transport in the barrier between the QW's. Since QW1 and QW2 have different well widths, the carrier lifetimes τ_w are different as well.[30,31] However, this effect is not dominant in the profiles. Since τ_w and τ_{rel} are determined separately, the transport effects can be separated from the carrier dynamics inside the QW's.

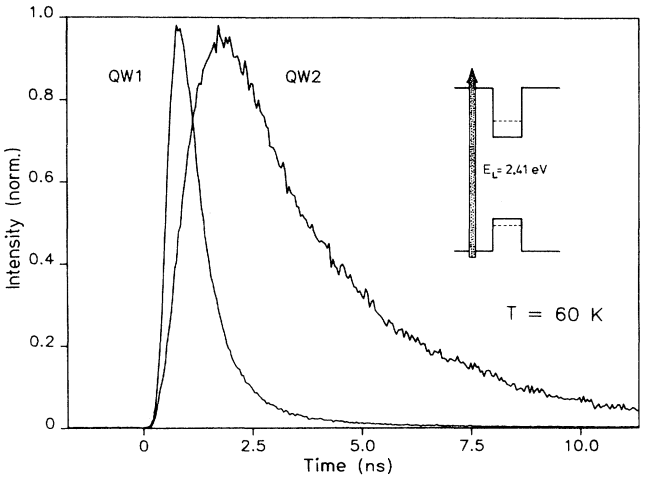

FIG. 5. Time-resolved emission of QW1 and QW2 for $T=60$ K for excitation energies that excite carriers mainly in the barriers.

Besides the generation of carriers at different distances from the probe layer (Fig. 4) or the comparison of the emission of two different QW's (Fig. 5) the transport in the barrier can be demonstrated most clearly by comparing samples of different barrier widths L_2. Figure 6 displays the emission of QW2 as a function of time for various barrier thicknesses in different samples. By increasing the distance L_2 between QW2 and the surface, the emission of QW2 is shifted to later times. Furthermore, we observe a broadening of the profiles with increasing L_2, indicating the influence of diffusive effects. In this diagram the sharpest profile corresponds to a total flight distance of $L_2=d_2=0.9$ μm (sample No. 2b). The

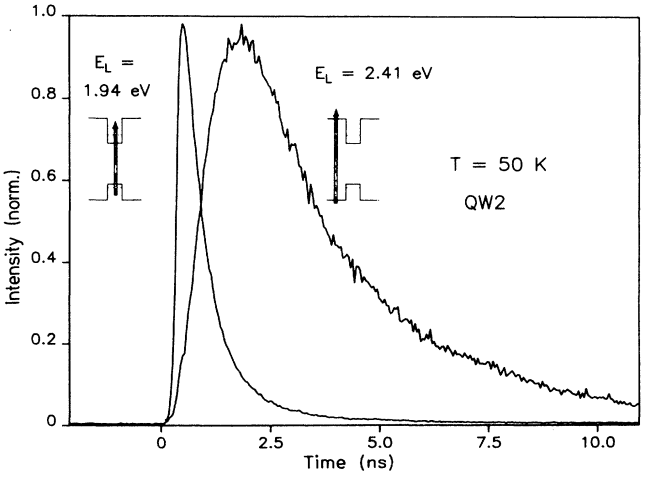

FIG. 4. Time-resolved emission of the second quantum well (QW2, located close to the substrate) for excitation energies absorbed only inside the QW's or mainly in the barriers (see insets).

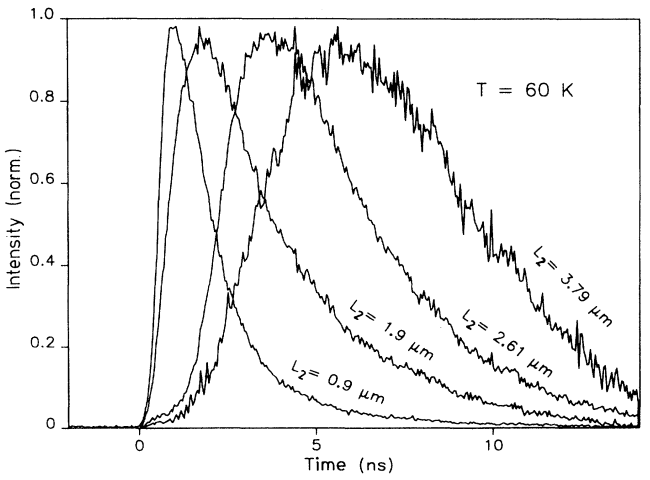

FIG. 6. Time-resolved emission of QW2 for different distances L_2 between the probe layer and the sample surface ($T=60$ K).

profiles which then appear in sequence for longer times are recorded for the samples No. 2 ($L_2=d_1+d_2=1.9$ μm), No. 1c ($L_2=d_2=2.61$ μm), and No. 1 ($L_2=d_1+d_2=3.79$ μm). The QW2 profiles of samples Nos. 1 and 2 also include the influence of the carrier trapping in QW1 which is located near the surface of the sample. This effect as well as the influence of surface recombination and the trapping of carriers by the substrate is considered in an ambipolar diffusion model presented below.

IV. THEORETICAL MODEL OF VERTICAL TRANSPORT

As can be seen from Figs. 3–6, the typical time scale for the transport in our structures is in the order of a few ns. This is much larger than the energy relaxation time of the photoexcited carriers in the barrier regions. Therefore, the influence of temperature gradients on the carrier transport can be neglected and a simple isothermal diffusion model is sufficient to describe the system. Furthermore, due to the strong electrostatic forces between the electrons and holes, the carrier pairs can be described as an effective one-component system and the ambipolar approximation can be used.[33] Hence, we describe the evolution of the carrier concentration by the one-dimensional continuity equation including a diffusion, a recombination, and a generation term:

$$\frac{\partial c}{\partial t}=D\frac{\partial^2 c}{\partial z^2}-\frac{c}{\tau_b}+g(z,t)\ . \tag{1}$$

D denotes the diffusivity and τ_b the lifetime of the carriers in the barrier. Since the aluminum content in the barrier material is 0.5, the band structure is indirect in $\mathbf{k}$ space. Thus, a carrier recombination in the barriers requires phonon assistance. This causes a carrier lifetime τ_b in the μs range. Hence, on the time scales considered here, the recombination term in Eq. (1) can be neglected. The term $g(z,t)$ describes the generation of the carriers by the laser pulse. We use a Gaussian shape in time with a full width at half maximum (FWHM) of $\Delta\tau$. For the spatial distribution we assume an exponential profile inside the sample caused by the characteristic absorption of the light described by the absorption coefficient α. Choosing $z=0$ at the sample surface we have

$$g(z,t)=g_0\exp\left[-\frac{t^2\times 4\ln 2}{\Delta\tau^2}\right]\exp(-\alpha z)\ . \tag{2}$$

Equation (1) describes the transport in the barrier material. Additionally, the properties of the surfaces and interfaces have to be considered. In many materials the probability of recombination is strongly enhanced at a surface.[11,34] This can be described by a surface recombination velocity s which relates the particle current density j to the carrier concentration c at the surface. In our samples, the interface between the third barrier d_3 and the substrate also acts as a surface since, due to the large band-gap discontinuities, no carrier can return from the substrate to the barrier region. Therefore, we have the two boundary conditions at the front surface,

$$j=-D\frac{\partial c}{\partial z}=-s_0 c \quad \text{for } z=0\ , \tag{3}$$

and for the interface between the third barrier d_3 and the substrate using L for the total barrier thickness $d_1+L_{z1}+d_2+L_{z2}+d_3$,

$$j=-D\frac{\partial c}{\partial z}=+s_L c \quad \text{for } z=L\ . \tag{4}$$

The consideration of the interface influence, i.e., the QW's in our structures, is more complicated. Since a fraction of the carriers is trapped into the QW's, the current densities on both sides in general will be different and each of the current densities j^{I} and j^{II} will depend on both carrier concentrations c^{I} and c^{II}, where I (II) denotes the value of the left- (right-) hand side of the interface. These current densities are given by the sum of diffusion and field currents. Since we consider an ambipolar system, the field current vanishes in our case. Using a linear relation between the current densities and the concentrations as in the case of surface recombination, we find that an interface can be described in general by four coefficients with the dimension of a velocity. For symmetry reasons due to identical barrier heights on both sides of the QW's in our case, the four coefficients reduce to two (the interface velocities s_A and s_B). The interface conditions are

$$j^{\mathrm{I}}=-D\frac{\partial c^{\mathrm{I}}}{\partial z}=+s_A c^{\mathrm{I}}-s_B c^{\mathrm{II}}\ , \tag{5}$$

$$j^{\mathrm{II}}=-D\frac{\partial c^{\mathrm{II}}}{\partial z}=+s_B c^{\mathrm{I}}-s_A c^{\mathrm{II}}\ . \tag{6}$$

In order to understand the meaning of these velocities, let us consider some properties of Eqs. (5) and (6).

The difference between the current densities on the left- and right-hand side of the QW is given by

$$j^{\mathrm{I}}-j^{\mathrm{II}}=(s_A-s_B)(c^{\mathrm{I}}+c^{\mathrm{II}})\ . \tag{7}$$

This difference describes the carriers that are captured by the QW. The velocity s_A-s_B can be interpreted as in "interface recombination velocity," analogous to the surface recombination velocity.

The velocity s_B is responsible for the coupling between both sides. $s_B=0$ corresponds to totally decoupled regions and Eqs. (5) and (6) reduce to the boundary conditions at the surfaces [see Eqs. (3) and (4)]. Finally, the limiting case $s_A=s_B$ with $s_A,s_B\to\infty$ leads to the condition $c^{\mathrm{I}}=c^{\mathrm{II}}$ and $j^{\mathrm{I}}=j^{\mathrm{II}}$ if the influence of the interface (here a QW) vanishes and the transport is purely bulklike.

In the following, the influence of QW's on the carrier motion in the barriers near a QW will be visualized. If the carriers move perpendicular to the heterointerface, some carriers are reflected, others are transmitted through the layer, and the rest is captured by the well. The transmission and reflection problem can be treated by quantum mechanics in a way very similar to the textbook problem of a "particle at a potential barrier." Since the carriers can move in positive and negative directions in this case, the problem has to include the formulation for both directions.

In Fig. 7 this is illustrated in the hydrodynamic approach for the electron potential well. The particle currents are indicated by arrows. The current density in each half-space is described by a part $j_{\rightarrow}$ which contains all carrier pairs moving in positive z direction and a part $j_{\leftarrow}$ which describes all carriers moving in the opposite direction. The current density in II which is directed in the positive z direction ($j^{\mathrm{II}}_{\rightarrow}$) is the sum of, first, the transmitted part of the total current in I initially moving in the positive z direction and of, second, the reflected part of the total current in II which flows in the negative z direction. For the current $j^{\mathrm{I}}_{\leftarrow}$ moving in I to the left we can formulate a similar equation. The difference between these currents and the appropriate initial currents is captured by the considered QW.

On a microscopic level the behavior of a carrier pair with wave vector $\mathbf{k}$ at an interface is determined by a set of probabilities: the probability of transmission from one side to the other $T(\mathbf{k})$, the probability of reflection into the same region $R(\mathbf{k})$, and the probability of a capture process $C(\mathbf{k})$, where, of course, the sum of all three probabilities has to be unity:

$$R(\mathbf{k})+T(\mathbf{k})+C(\mathbf{k})=1 \ . \tag{8}$$

Using these probabilities (and Fig. 7), the current densities can be formulated in the different areas for both directions (ingoing and outgoing),

$$j^{\mathrm{I}}_{\leftarrow}=\bar{R}j^{\mathrm{I}}_{\rightarrow}+\bar{T}j^{\mathrm{II}}_{\leftarrow} \ , \tag{9}$$

$$j^{\mathrm{II}}_{\rightarrow}=\bar{R}j^{\mathrm{II}}_{\leftarrow}+\bar{T}j^{\mathrm{I}}_{\rightarrow} \ . \tag{10}$$

$\bar{R}$ and $\bar{T}$ denote the reflection and transmission probabilities averaged with respect to the distribution function. Under the assumption that the distribution function of the incoming carriers can be approximated by an undisturbed Maxwellian, the interface velocities can be expressed according to Eqs. (9) and (10) as follows:[13]

$$s_A=\sqrt{kT/2\pi m_b}(\bar{T}+\bar{C}) \ , \tag{11}$$

$$s_B=\sqrt{kT/2\pi m_b}(\bar{T}) \ . \tag{12}$$

Hence, we are able to describe a QW with two boundary conditions combining the carrier concentrations and their spatial derivative on both sides of the QW using two velocity parameters. The velocity s_A includes the probability $(1-\bar{R})$ thus describing all unreflected carriers. The velocity s_B includes the probability $\bar{T}$ which describes all transmitted carriers.

In previous publications[13,17] we investigated in detail the microscopic probabilities of the case of capture by emission of optical phonons. Using quantum-mechanical reflection above the barrier energy, we obtain resonances leading to a strong dependence on the QW width. For isothermal transport we have shown that the carrier concentration calculated as a function of time in the position of QW—this solution was found by a numerical approach based on the Boltzmann equation including the microscopic probabilities—is in very good agreement with solutions of the diffusion equation using the interface velocities calculated according to Eqs. (11) and (12).

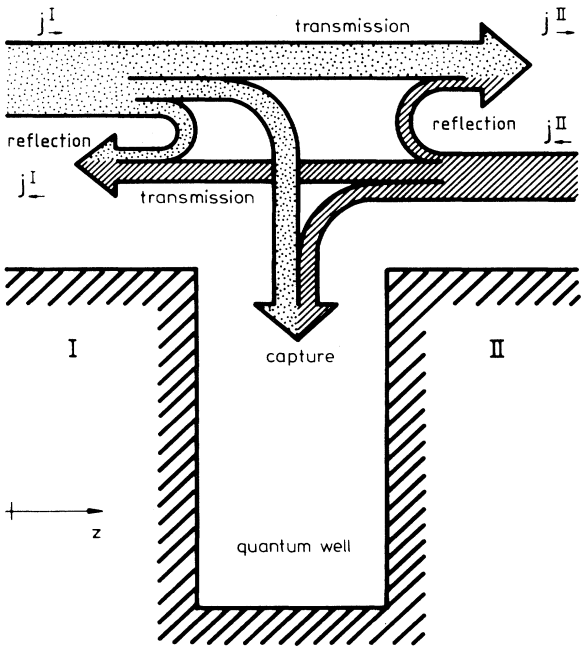

FIG. 7. Schematic design of our model used for the description of the influence of quantum wells on carrier transport in the barrier material. The boundary conditions are illustrated in this example for the electron potential well. Bottom: conduction-band structure; top: corresponding current densities.

V. DETERMINATION OF TRANSPORT PROPERTIES AND TRAPPING PARAMETERS

In this section line-shape fits are used to extract diffusivities, surface and interface recombination velocities from the experimental profiles as well as characteristic properties that describe the trapping behavior of QW's. For the numerical solution of the vertical transport problem of the double-QW structures used for our measurements, the differential equation (1) is solved in consideration of the boundary conditions [Eqs. (3)–(6)].

At a given temperature the transport profiles are fitted with the same set of residual parameters (D,s_i) for all samples obtained from the same as-grown sample. The surface recombination velocity s_0 is the only parameter that may be different between the as-grown samples and the etched samples. The diffusivity D and the parameters τ_{w1}, τ_{w2}, τ_{rel1}, τ_{rel2}, s_{A1}, s_{B1}, s_{A2}, s_{B2}, and s_L are expected not to change during the etching process since they describe processes spatially well separated from the surface.

Figure 8 displays the emission of QW's located at various distances from the sample surface as a function of time (transport profiles) together with line-shape fits. The experimental profile of QW1 is given by triangles and the profiles of QW2 are plotted by circular symbols. The first (left-hand side) and the fourth (right-hand side) profile are

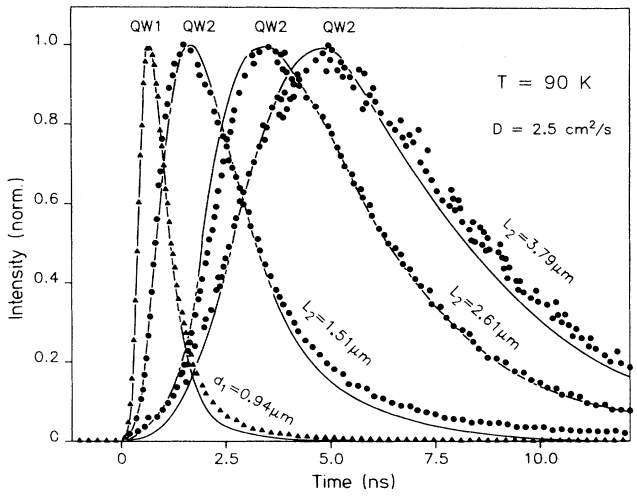

FIG. 8. Time-resolved emission of QW1 (triangles) and QW2 (circles) for different distances from the sample surface (d_1, L_2). For $T=90$ K the best line-shape fits are indicated by solid lines and yield a diffusivity of $D=2.5$ cm^2/s.

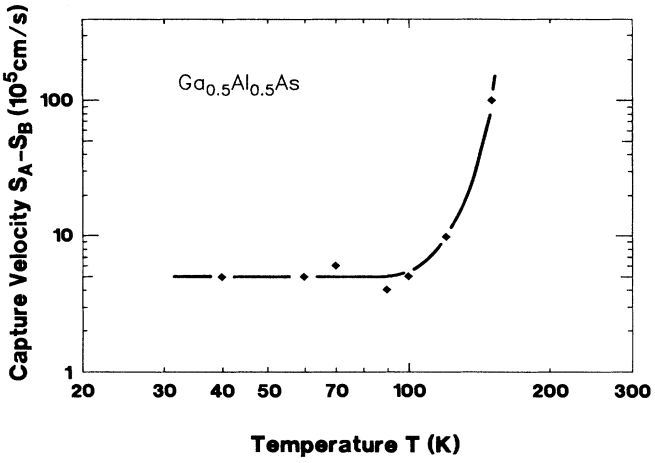

FIG. 9. Temperature dependence of the difference of the two velocities $s_A - s_B$, which is proportional to the probability of carrier capture into the QW. The solid line is drawn to guide the eye.

associated with the as-grown sample No. 1. The second and third profiles were measured using the structures Nos. 1e and 1d, respectively. The solid lines represent fits by the model developed in Sec. III. For $T=90$ K, e.g., the experimental profiles of the whole set of samples are described best using a diffusivity of 2.5 cm^2/s. For the velocity parameters we find for $T=90$ K, $s_{A1}=s_{A2}=s_0=s_L \gtrsim 10^7$ cm/s and $s_{A1}-s_{B1}=s_{A2}-s_{B2}=4\times10^5$ cm/s.

The high values of the surface recombination velocity s_0 and the interface recombination velocity s_L indicate efficient carrier capture at $z=0$ and L, respectively. Note that nearly no difference can be observed in the calculated profiles between $s_{0,L} > 10^7$ cm/s and $s_{0,L}=\infty$. Thus, all carriers seem to be captured by the surface or by the interface to the substrate in these cases. Additionally, the reflection of carriers by the QW's seems to be negligible since the velocities s_{A1} and s_{A2}, describing all carriers that are not reflected, range on the order of 10^7 cm/s. Figure 9 displays the difference $(s_{Ai}-s_{Bi})$ as a function of temperature. According to (7) the difference of the velocities $s_{Ai}-s_{Bi}$ describes the probability of carrier capture into the QW "i" showing no measurable variation with temperature below 100 K in Fig. 9. In order to obtain an estimate of the capture probability from the velocities $s_{Ai}-s_{Bi}$, we have to compare the velocity difference with typical values of the carrier transit velocity in the region of the QW's. The low-temperature data in Fig. 9 correspond to a capture probability in the percent range that increases close to 1 at high temperatures. This is in agreement with the observed strong decrease of the time-integrated emission intensity of QW2 with increasing temperature above $T=100$ K. The reason is most likely the efficient capture of carriers by QW1 so that only few carriers reach QW2. In contrast to the velocity difference $(s_{Ai}-s_{Bi})$ no temperature dependence is observed for the velocities s_{Ai}, s_0, and s_L within the experimental error. These values are already so high that a further increase would not affect the profiles. Furthermore, the evaluation of our experimental data yields no difference in $(s_{Ai}-s_{Bi})$ between QW1 and QW2.

In Fig. 10 the diffusivity is presented as a function of temperature in a double-logarithmic diagram. In the range between 40 and 150 K we observe a slight increase of the diffusivity with rising temperature. A fit based on a power law dependence of the diffusivity on temperature is performed in the temperature range $40 \le T \le 120$ K and yields $D \sim T^{0.5}$ (straight line). Due to the low carrier concentrations in the barriers, the Einstein relation $\mu(T)=eD(T)/kT$ can be used in a good approximation to calculate the ambipolar mobility. This yields a temperature dependence for the mobility of $\mu \sim T^{-0.5}$ in the temperature range $40 \le T \le 120$ K as shown by the solid

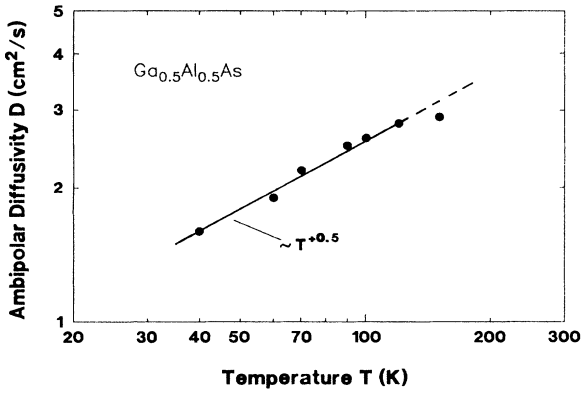

FIG. 10. Ambipolar diffusivities as a function of temperature. The solid line is a fit to the experimental data, based on a power law for the temperature dependence.

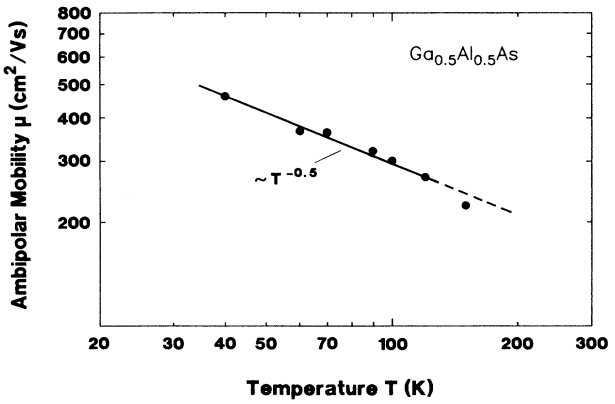

FIG. 11. Ambipolar mobilities as a function of temperature. The solid line as well as the mobility values are calculated from Fig. 10 using the Einstein relation.

line in Fig. 11. The temperature dependence is due most probably to alloy-disorder scattering processes in the $Al_{0.5}Ga_{0.5}As$ barriers since we obtain exactly the theoretical temperature dependence.[35] For higher temperatures we observe a smaller mobility as indicated by the dashed line in Fig. 11. This is probably due to a contribution of acoustic-deformation-potential scattering and polar-optical scattering. Acoustic-deformation-potential scattering as well as polar-optical scattering yield a stronger temperature dependence of the mobility in 3D ambipolar systems[30] than alloy-disorder scattering. Due to the temperature variation and the absolute values of the scattering rates the polar-optical scattering dominates for higher temperatures.

For a given temperature the ambipolar diffusivity in the barriers has the same value within the experimental error for all samples investigated. The absolute values for our experimental ambipolar mobility (e.g., $\mu=330$ $cm^2/V\,s$ at $T=90$ K) and $x_{Al}=0.5$ are slightly lower than theoretical values calculated for the three-dimensional alloy-disorder scattering ($\mu_h \sim 650$ $cm^2/V\,s$ and $\mu_e \sim 2200$ $cm^2/V\,s$).[36,37] Our experimental ambipolar mobility values determined in our experiment are in good agreement with ambipolar mobility values that we calculated from experimental unipolar Hall data[38] in $Al_{0.5}Ga_{0.5}As$.

The shape of the calculated profiles used for the lineshape fits is very sensitive to the geometry of the structure (d_1, d_2, d_3). Comparing the calculated profiles of QW1 in structures Nos. 2 and 1 (i.e., $d_2=2.83$ μm, respectively) we find that the profiles of QW1 are also influenced by carriers diffusing back from the second barrier d_2 to QW1. Note that in these samples the first barrier layer d_1 is of identical thickness. The diffusion from the barrier layer d_2 back to QW1 is much more efficient in structure No. 1 compared to No. 2 due to a more extended layer d_2. This causes a slower decrease of the QW1 transport profile in No. 1 compared to No. 2.

VI. CONCLUSION

In this paper experimental results as well as a detailed model of ambipolar transport in semiconductor heterostructures are presented. A high-resolution TOF method using two QW's has been applied to probe the carrier transport perpendicular to the heterointerfaces. Ambipolar diffusivities, mobilities as well as surface and interface recombination velocities, were determined in a large set of different $GaAs/Al_{0.5}Ga_{0.5}As$ structures as a function of temperature. We developed a detailed model to describe the influence of boundary conditions on vertical ambipolar transport in heterostructures, and found surface and interface recombination to be crucial. In addition, our evaluation provides insight in the carrier capture from barrier layers into quantum wells. Between 40 and 120 K, alloy-disorder scattering is found to limit the ambipolar mobilities in the $Al_{0.5}Ga_{0.5}As$ barrier layers of our samples. For higher temperatures the ambipolar mobilities are also influenced by acoustic-deformation-potential scattering and polar-optical scattering.

ACKNOWLEDGMENTS

We wish to thank M. Pilkuhn and G. Mayer for helpful discussions and R. Germann for dry etching of several samples. The financial support of this study by the Stiftung Volkswagenwerk and the Deutsche Forschungsgemeinschaft (SFB329) is gratefully acknowledged.

*Permanent address: Deutsche Bundespost TELEKOM, Forschungsinstitut beim FTZ, Postfach 100003, D-6100 Darmstadt, Germany. Present address: NTT Opto-electronic Laboratories, Integrated Opto-electronic Laboratories, 3-1 Morinosato Wakamiya, Atsugi-shi, Kanagawa Pref. 243-01 Japan.

†Permanent address: Technische Physik, Universität Würzburg, Am Hubland, D-8700 Würzburg, Germany.

‡Present address: Dipartimento di Fisica, Università di Modena, Via Campi 213/A, I-41100 Modena, Italy.

[1]B. F. Levine, W. T. Tsang, C. G. Bethea, and F. Capasso, Appl. Phys. Lett. **41**, 470 (1982).

[2]J. F. Palmier, C. Minot, J. L. Lievin, F. Alexandre, J. C. Harmand, J. Dangla, C. Dubon-Chevallier, and D. Ankri, Appl. Phys. Lett. **49**, 1260 (1986).

[3]R. K. Ahrenkiel, D. J. Dunlavy, H. C. Hamaker, R. T. Green, C. R. Lewis, R. E. Hayes, and H. Fardi, Appl. Phys. Lett. **49**, 725 (1986); R. K. Ahrenkiel, D. J. Dunlavy, D. Greenberg, J. Schlupmann, H. C. Hamaker, and H. F. MacMillan, *ibid.* **51**, 776 (1987)

[4]B. Deveaud, A. Chomette, B. Lambert, A. Regreny, R. Romestain, and P. Edel, Solid State Commun. **57**, 885 (1986).

[5]H. Hillmer, G. Mayer, A. Forchel, K. S. Löchner, and E. Bauser, Appl. Phys. Lett. **49**, 948 (1986); in *High-Speed Elec-*

tronics, Springer Series in Electronic and Photonics Vol. 22, edited by D. H. Auston, B. Källback, and H. Beneking (Springer, Berlin, 1986) p. 97.

[6]B. Devaud, J. Shah, T. C. Damen, B. Lambert, and A. Regreny, Phys. Rev. Lett. **58**, 2582 (1987).

[7]D. J. Westland, D. Mihailovic, J. F. Ryan, and M. D. Scott, Appl. Phys. Lett. **51**, 590 (1987).

[8]J. Benhal, P. Lavallard, C. Gourdon, R. Cruosson, M. L. Roblin, A. M. Pougnet, and R. Planel, J. Phys. (Paris) Colloq. Suppl. **48**, C5-471, (1987).

[9]B. Devaud, J. Shah, T. C. Damen, B. Lambert, A. Chomette, and A. Regreny, IEEE J. Quantum Electron. **24**, 1641 (1988).

[10]B. Lambert, B. Davaud, A Chomette, A. Regreny, and B. Sermage, Superlatt. Microstruct. **5**, 565 (1989).

[11]T. Kuhn and G. Mahler, Phys. Rev. B **40**, 12 147 (1989).

[12]T. Kuhn and G. Mahler, Phys. Rev. B **35**, 2827 (1987).

[13]T. Kuhn and G. Mahler, Solid-State Electron. **32**, 1851 (1989).

[14]S. V. Kozyrev and A. Ya Shik, Fiz. Tekn. Poluprovodn. **19**, 1667 (1985) [Sov. Phys. Semicond. **19**, 1024 (1985)].

[15]J. A. Brum, and G. Bastard, Phys. Rev. B **33**, 1420 (1986).

[16]H. Schichijo, R. M. Kolbas, N. Holonyak, R. D. Dupuis, and P. D. Dapkus, Solid State Commun. **27**, 1029 (1987).

[17]T. Kuhn and G. Mahler, Phys. Scr. **38**, 216 (1988).

[18]Y. Muruyama, Phys. Rev. B **34**, 2500 (1986).

[19]J. Feldmann, G. Peter, E. O. Göbel, K. Leo, H.-J. Polland, K. Ploog, K. Fujiwara, and T. Nakayama, Appl. Phys. Lett. **51**, 226 (1987).

[20]H.-J. Polland, K. Leo, K. Rother, K. Ploog, J. Feldmann, G. Peter, E. O. Göbel, K. Fujiwara, T. Nakayama, and Y. Ohta, Phys. Rev. B, **38**, (1988).

[21]J. A. Brum, T. Weil, J. Nagle, and B. Vinter, Phys. Rev. B **34**, 2381 (1986).

[22]Y. C. Chen, R. G. Waters, J. J. Coleman, D. P. Bour, and P. Wang, Proceedings of the 125th International Semicondor Laser Conference, Davos, 1990 [IEEE J. Quantum Electron. (to be published)].

[23]B. Deveaud, F. Clérot, A. Regreny, K. Fujiwara, K. Mitsunaga, and J. Ohta, Appl. Phys. Lett. **55**, 2646 (1989).

[24]A. Weller, P. Thomas, J. Feldmann, G. Peter, and E. O. Göbel, Appl. Phys. A **48**, 509 (1989).

[25]E. O. Göbel, H. Jung, J. Kuhl, and K. Ploog, Phys. Rev. Lett. **51**, 1588 (1983).

[26]D. Bimberg, J. Christen, A. Steckenborn, G. Weimann, and W. Schlapp, J. Lumin. **30**, 562 (1985).

[27]E. Eisenstein, J. M. Wiesenfield, M. Wegener, U. Koren, D. S. Chemla, and G. Raybon, Proceedings of the 12th International Semiconductor Laser Conference, Davos, 1990 (Ref. 22).

[28]B. Monemar, K. K. Shih, and G. D. Pettit, J. Appl. Phys. **47**, 2604 (1976).

[29]D. E. Aspnes, S. M. Kelso, R. A. Logan, and R. Bhat, J. Appl. Phys. **60**, 754 (1986).

[30]H. Hillmer, A. Forchel, S. Hansmann, M. Morohashi, E. Lopez, H. P. Meier, and K. Ploog, Phys. Rev. B **39**, 10 901 (1989).

[31]J. Feldmann, G. Peter, E. O. Göbel, P. Dawson, K. Moore, C. Foxon, and R. J. Elliot, Phys. Rev. Lett. **59**, 2337 (1987).

[32]H. Hillmer, A. Forchel, R. Sauer, and C. W. Tu, Phys. Rev. B **42**, 3220 (1990).

[33]H. Hillmer, T. Kuhn, B. Laurich, A. Forchel, and G. Mahler, Phys. Scr. **35**, 520 (1987).

[34]G. Mahler, T. Kuhn, A. Forchel, and H. Hillmer, in *Optical Nonlinearities and Instabilities in Semiconductors,* edited by H. Haug, (Acadamic, San Diego, 1988), p. 159.

[35]B. R. Nag, in *Electron Transport in Compound Semiconductors,* edited by H.-J. Queisser, Springer Series in Solid-State Sciences Vol. 11 (Springer, Berlin, 1980).

[36]K. Masa, E. Tokumitsu, E. Konagai, and K. Takahashi, J. Appl. Phys. **54**, 5785 (1983).

[37]A. K. Saxena and K. S. Gurumurthy, J. Phys. Chem. Solids **43**, 801 (1982).

[38]C. T. Choi, and J. J. Lee, J. Appl. Phys. **64**, 4993 (1988).